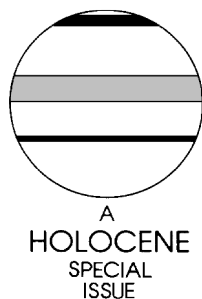


Effects of mid-Holocene river runoff on the Arctic ocean/sea-ice system: a numerical model study

Matthias Prange* and Gerrit Lohmann

(University of Bremen, Geosciences Department, PO 330 440, D-28334 Bremen, Germany)



Abstract: Recent geological studies have revealed that the freshwater input to the Arctic Ocean was highly variable during the Holocene. In the present study, the influence of mid-Holocene river runoff on large-scale Arctic ocean/sea-ice dynamics is examined using a general circulation model. A palaeohydrological forcing for the time interval around 6 ka BP (^{14}C timescale) is constructed by compiling data from the available literature. Keeping all other forcing fields and bottom topography of the ocean model at present-day values, the effect of a changed freshwater input to the Arctic Ocean is isolated. The model shows that freshwater supply is vitally important for the polar oceanic circulation. In particular, a close connection between Siberian river runoff and the path of the Transpolar Drift (TPD) is found. Consistent with palaeoceanographic findings of driftwood delivery to the Canadian Arctic Archipelago and Baffin Bay, the model results suggest that enhanced freshwater discharge during the mid-Holocene caused an eastward shift of the TPD with strengthened outflow through Fram Strait.

Key words: Ocean/sea-ice modelling, Arctic river runoff, Arctic palaeoceanography, Transpolar Drift, Holocene.

Introduction

The Arctic Ocean is unique among all oceans because its hydrographical characteristics are profoundly influenced by a large input of fresh water from the surrounding continents (e.g., Aagaard and Carmack, 1989). Relative to its size, the Arctic Ocean receives the largest river-water input of all oceans (Grabs *et al.*, 1996). Since the thermal expansion coefficient of sea water is very small at low temperatures, the density of cold polar water masses is primarily a function of salinity. Therefore, river inflow into the Arctic Ocean controls density-driven dynamics and stratification. In particular, the formation of a cold halocline depends on river runoff (Rudels *et al.*, 1996; Steele and Boyd, 1998). The cold halocline, an isothermal near freezing-point layer located at 50–150 m depth over most parts of the Arctic basins, effectively shields the surface from heat stored at intermediate depths in the Atlantic layer. It is therefore of utmost importance for the Arctic sea-ice cover which, in turn, acts as a natural refrigerator for the planet due to its high albedo.

Geological records indicate that the basic features of today's Arctic Ocean circulation have been existent throughout the Holocene: inflowing Atlantic water through Fram Strait and the Barents Sea (e.g., Cronin *et al.*, 1995; Stein and Fahl, 2000; Boucsein, 2000; Lubinski *et al.*, 2001), a Transpolar Drift (e.g., Dyke *et al.*, 1997; Behrends, 1999) and an anticyclonic gyre in the western Arctic (e.g., Behrends, 1999). However, there are also

geological evidences for variations in the strength of the currents on a century-to-millennium timescale. Moreover, shifts in their positions seem to have occurred (e.g., Dyke *et al.*, 1997). It has been speculated that long-term variations in the Arctic Ocean flow pattern were caused mainly by changes in the wind-stress field (e.g., Tremblay *et al.*, 1997). The role of freshwater forcing in Arctic Ocean Holocene variability has not been studied so far. Recent geological studies, however, point to a considerable variability of the hydrological cycle in the Arctic region with changing river-water fluxes into the polar seas throughout the Holocene (e.g., Kunz-Pirrung, 1998; Boucsein, 2000; Andreev and Klimanov, 2000).

Numerical modelling may help to improve our understanding of the Arctic ocean/sea-ice system. In the present study, we examine the influence of mid-Holocene Arctic river discharge on large-scale ocean/sea-ice dynamics by means of a general circulation model of the Arctic Ocean, the Nordic Seas and the North Atlantic. In order to force the model, we construct a circum-Arctic palaeoriver discharge pattern for the time interval around 6 ka BP (^{14}C timescale) during the Atlantic stage by compiling palaeohydrological data from the available literature. Keeping all other forcing fields and bottom topography of the ocean model at present-day values, we isolate the effect of a changed freshwater input to the Arctic Ocean. Comparing the results of the model forced by present-day freshwater fluxes with the palaeohydrological model run directly reveals the dynamical impact of mid-Holocene freshwater forcing.

*Author for correspondence (e-mail: mprange@palmod.uni-bremen.de)

Present-day and mid-Holocene Arctic river runoff

In the following, we briefly describe modern Arctic river runoff and summarize geological studies concerning the freshwater input during the Atlantic stage. The observed and reconstructed freshwater fluxes shall serve as a forcing for the ocean/sea-ice model, which is described afterwards.

Modern runoff

Today, the freshwater balance of the Arctic Ocean is dominated by river runoff (e.g., Aagaard and Carmack, 1989). About $3200 \text{ km}^3 \text{ yr}^{-1}$ of river water flows directly into the Arctic Ocean. Around 60% of this fresh water is provided by the four largest Arctic rivers, namely Yenisey, Lena, Ob and Mackenzie (Figure 1). In addition, about $380 \text{ km}^3 \text{ yr}^{-1}$ of freshwater discharged along the Norwegian coast is advected into the Arctic Ocean by the Norwegian Coastal Current. Arctic river runoff is characterized by a marked seasonality with maximum discharge in spring/early summer, and almost vanishing outflow during the winter months. Some rivers, like the Lena River, discharge more than 85% of their annual outflow between May and September. The influence of human activities on the discharge of Arctic rivers is (still) negligible (Vuglinsky, 1997). Figure 1 shows the locations of Arctic rivers with an annual outflow of more than $30 \text{ km}^3 \text{ yr}^{-1}$.

Mid-Holocene runoff

Compiling geological data from various sources, we estimate circum-Arctic palaeoriver discharge for the mid-Holocene. Cheddadi *et al.* (1997) reconstructed $P-E$ (precipitation minus evapotranspiration) across Europe for 6 ka BP from pollen data using the modern pollen analogue technique constrained with lake-level data. Their results suggest that $P-E$ over Norway was $5-25 \text{ cm yr}^{-1}$ less than at present, while $P-E$ was $10-15 \text{ cm yr}^{-1}$ greater in eastern Europe. Integrating over the corresponding drainage areas, we can roughly estimate a decreased runoff into the Norwegian Sea by about 25%, and a 25% increase of freshwater input to the Barents Sea.

Recent studies on the distribution of aquatic palynomorphs in marine Holocene sediments have provided valuable information

about hydrographic changes and freshwater inflow variability in the Kara and Laptev Seas. Boucsein (2000) analysed the concentration of freshwater algae (chlorococcalean algae, such as *Pediastrum* and *Botryococcus*) in sediment cores from different locations in the Kara Sea and along the Eurasian continental margin. For 6 ka BP, the record indicates a slightly decreased freshwater input to the Kara Sea. This finding is corroborated by records of foraminifer distributions and diatom assemblages from that region (Polyak *et al.*, 2000; 2002). A quantification of the runoff variability, however, is difficult. Here we assume a reduction of 25% relative to present-day values.

Kunz-Pirrung (1998) investigated the distribution of aquatic palynomorphs in recent and Holocene sediments from the Laptev Sea shelf. A strong influx of river water into the eastern Laptev Sea between 5.5 and 6.7 ka BP is indicated by high concentrations of chlorococcalean algae. The author estimates a maximum freshwater discharge for the time around 6.4 ka BP which was probably twice as high as today. This estimate is consistent with a bioclimatic vegetation model (Monserud *et al.*, 1998), which shows large precipitation anomalies in East Siberia during the Atlantic stage. The annual precipitation over Yakutia was more than 20 cm (i.e., about two times) greater than today.

As to the continental runoff from the East Siberian and North American coasts, we refer to older reconstructions by Belyaev and Georgiadi (1992). Utilizing palaeofloristic data and climatic indicators, they reconstructed spatial patterns of runoff for the mid-Holocene. The results suggest a slightly larger freshwater input to the East Siberian Sea, and North American runoff close to the present one. Integration over the eastern Siberian catchment area yields a 25% increase of freshwater discharge into the East Siberian Sea.

Model description and experimental design

Ocean/sea-ice model and forcing

In order to examine the effects of freshwater discharge on high-latitude ocean dynamics, we utilize a coupled ocean/sea-ice model. The ocean model is set up on the base of the hydrostatic

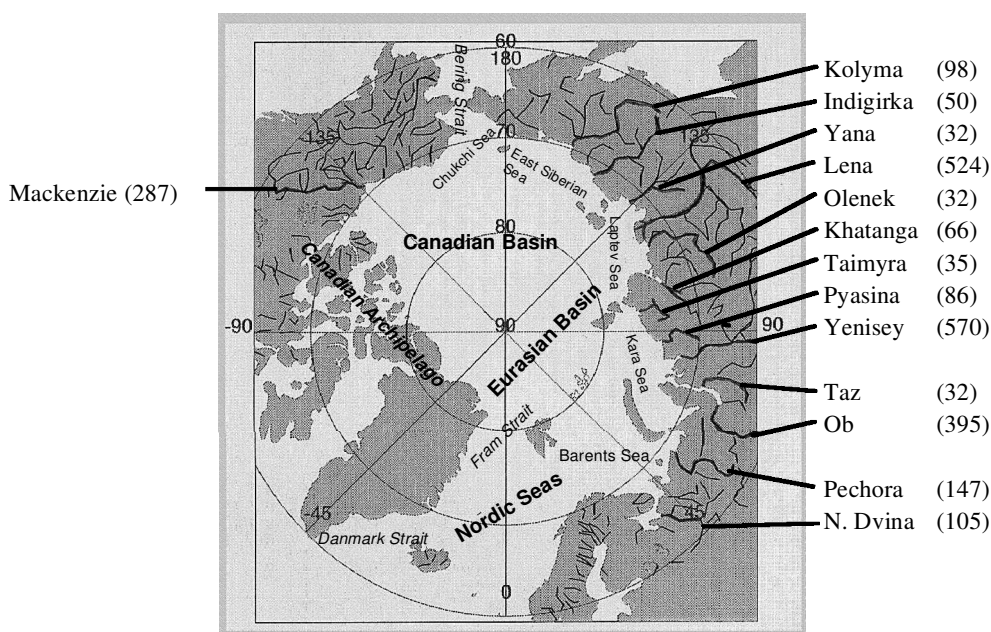


Figure 1 Arctic rivers implemented in the model and their mean discharge (in $\text{km}^3 \text{ yr}^{-1}$). Values for Taimyra and Pyasina are taken from Treshnikov (1985). For all other rivers, the flow into the ocean was calculated based on gauged discharge data, provided by the Global Runoff Data Centre (GRDC) at the Federal Institute of Hydrology, Koblenz, Germany.

Geophysical Fluid Dynamics Laboratory (GFDL) primitive equation model MOM-2 (Pacanowski, 1995). An open-surface formulation, based on the implicit free-surface method by Dukowicz and Smith (1994), allows for dynamic surface elevation and volume fluxes due to precipitation, evaporation and river runoff. Melting and freezing of sea ice is included as a salt flux, where the salinity of sea ice is set to 3 psu. This treatment of surface freshwater fluxes is similar to the approach used by Tartinville *et al.* (2001). The ocean/sea-ice model is fully prognostic, i.e., no diagnostic or restoring terms are added to the conservation equations.

The model domain spans the Arctic Mediterranean (i.e., the Arctic Ocean proper and the Nordic Seas) and the Atlantic Ocean north of approximately 20°S. The model is formulated on a rotated grid to avoid the singularity of geographical coordinates at the pole (Figure 2). It has a horizontal resolution of about 100 km and 19 non-equidistant levels in the vertical. Using the flux-corrected transport (FCT) algorithm (Zalesak, 1979; Gerdes *et al.*, 1991) for tracer advection, explicit diffusion is set to zero. The ocean model is coupled to a dynamic-thermodynamic sea-ice model with viscous-plastic rheology, which is defined on the same horizontal grid (Harder, 1996). A time step of 45 minutes is used for all prognostic quantities of the coupled model.

Monthly varying inflow of Pacific water through Bering Strait is implemented based on direct measurements by Roach *et al.* (1995). The salinity of this inflow varies between 31.5 psu in September/October and 33.5 psu in March/April. The mean volume flux is 0.8 Sv (1 Sv = 1 Sverdrup = $10^6 \text{ m}^3 \text{ s}^{-1}$), but seasonal variability is considerable. Minimum fluxes in December and March are 0.3 Sv, while the maximum flux in September amounts to 1.3 Sv. The Bering Strait inflow is associated with a heat supply during the summer months. The temperature rises to 4°C in September, while winter temperatures (December–May) are at freezing for the salinity.

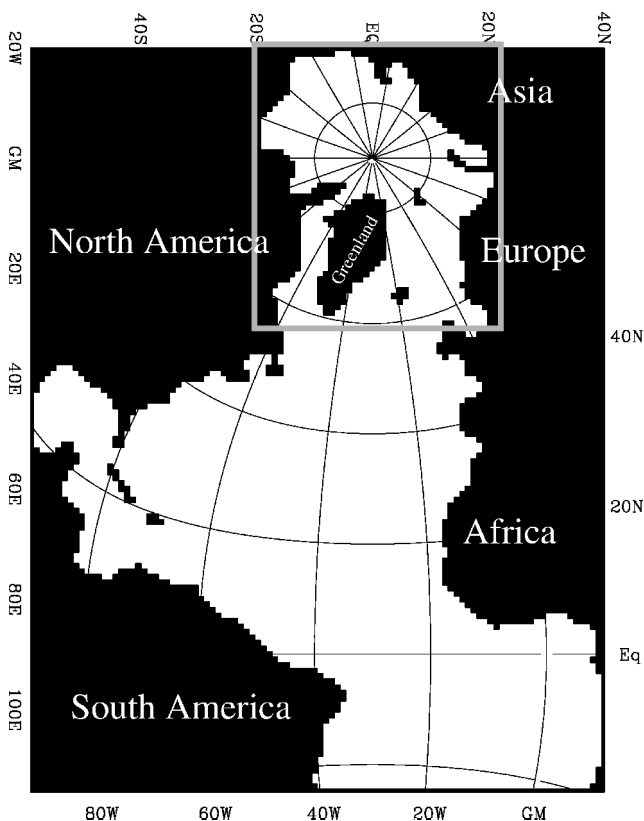


Figure 2 Domain of the model. The model equations are defined on a rotated grid. Both the geographical and the model grid coordinates are displayed. The frame marks the area that is shown in Figures 3–5.

The ocean/sea-ice model is forced by atmospheric fields, comprising 2 m-temperature, 2 m-dewpoint temperature, cloud cover, precipitation, wind speed and wind stress. Except for daily wind stress, all forcing fields are monthly varying. The atmospheric fields are derived from a validated 15-year (1979–93) set of assimilated data provided by the reanalysis project of the European Center for Medium-Range Weather Forecasts (ECMWF). The data have been processed to construct a ‘typical’ year, i.e., a mean annual cycle with daily wind stress fluctuations superimposed (Roeske, 2001).

In addition to atmospheric forcing and Bering Strait inflow, the ocean/sea-ice system is forced by river runoff, which is implemented as a zero-salinity mass flux into the ocean model’s topmost level. For the Atlantic portion of the model domain, the eight largest rivers are included as well as the freshwater supply from Hudson Bay and the Baltic Sea. Runoff from the Norwegian coast enters the Nordic Seas. The treatment of Arctic rivers is described below.

Experiments

Two experiments are performed, differing in river discharge into the Arctic Ocean. The discharge distributions refer to the present-day situation (experiment PD) and to the time around 6 ka BP during the mid-Holocene (experiment MH).

A climatology for monthly discharge of the largest Arctic rivers (displayed in Figure 1) has been constructed to force the model in experiment PD. Based on various estimates (Plitkin, 1978; AANII, 1990; Vuglinsky, 1997) some ungauged runoff is added during summer (June–September). Along the coastlines of the Barents, Kara and Laptev Seas an additional freshwater inflow of $520 \text{ km}^3 \text{ yr}^{-1}$ is equally distributed. Ungauged runoff from the eastern Siberian, North American and northern Greenland coasts is smaller: a total of $180 \text{ km}^3 \text{ yr}^{-1}$ is added in these regions. In order to detect the pathways of river water in the Arctic Ocean, a passive tracer is implemented in the model, the value of which is set to 1 for inflowing water from gauged and ungauged Arctic runoff.

To create a freshwater forcing for the Arctic Ocean in experiment MH, the changes in runoff as described in the previous section are taken into account: runoff from the Norwegian coast as well as into the Kara Sea is 25% lower than today, whereas the freshwater fluxes into the Barents and East Siberian Seas are enhanced by 25%. The largest change occurs in the Laptev Sea. Here, the total river discharge is doubled. To implement these changes in the ocean model, we increase/decrease the modern freshwater input to each coastal grid cell at each time step by the respective percentage.

The freshwater forcing for the two experiments is summarized in Table 1.

Table 1 Freshwater input from continents to the Arctic Ocean for the present-day experiment PD and the mid-Holocene experiment MH (units are $\text{km}^3 \text{ yr}^{-1}$)

| Region | Present-day (PD) | Mid-Holocene (MH) |
|---------------------------------------|------------------|-------------------|
| Norwegian coast | 380 | 285 |
| Barents Sea | 452 | 565 |
| Kara Sea | 1310 | 983 |
| Laptev Sea | 797 | 1594 |
| East Siberian Sea | 195 | 244 |
| North American/North Greenland coasts | 405 | 405 |
| Total | 3539 | 4076 |

Results

For a direct comparison of the results, the experiments PD and MH are started from the same initial conditions. The initial state is taken from a spin-up run described by Prange (2003). The river-water tracer is set to 0 everywhere in the ocean. For each experiment the model is integrated 60 years. This timespan corresponds to about six times the mean residence time of present-day Arctic halocline waters (Schlosser *et al.*, 1999).

Present-day circulation and hydrography (experiment PD)

Experiment PD is aimed at simulating the present-day circulation. In the following, we show annual mean fields from the last year of the integration period.

The ocean circulation averaged over the top 80 m in the polar and subpolar seas is shown in Figure 3a. The top 80 m are represented by the three topmost levels of the model grid and comprise the surface mixed layer with the upper part of the cold halocline in the Arctic Ocean. The model captures the characteristic features of the observed flow pattern markedly well. A strong cyclonic gyre dominates the Nordic Seas, consisting of the EGC (East Greenland Current) in the west and the NAC (Norwegian Atlantic Current) in the east. The latter transports warm water from the Atlantic to the north, while the EGC carries cold and fresh polar water to the south, where it leaves the Nordic Seas through Denmark Strait. Atlantic water enters the Barents Sea, bringing some heat into the Arctic Ocean. This current constitutes the southern branch of an overall cyclonic flow pattern in the eastern Arctic Ocean. The Canadian Basin in the western Arctic is dominated by the anticyclonic Beaufort Gyre. The western anticyclonic gyre meets the eastern cyclonic circulation in the central Arctic, thereby forming the current system of the Transpolar Drift (TPD). The TPD carries polar waters towards the outlets of the Arctic Ocean, namely Fram Strait and Nares Strait (Canadian Archipelago).

The mean ice drift resembles the upper ocean circulation, with an anticyclonic gyre over the Canadian Basin, a TPD, outflow through Fram Strait and an EGC (indicated schematically by arrows in Figure 3b). The distribution of modelled sea ice shows a typical pattern that is well known from other model studies (e.g., Hibler, 1979; Chapman *et al.*, 1994; Harder, 1996; Zhang *et al.*, 1999) and which is consistent with sonar data (e.g., Hibler, 1979; Bourke and Garrett, 1987; Bourke and McLaren, 1992). This pat-

tern is characterized by maximum ice thickness north of Canada, an ice thickness of 3–4 m near the pole and relatively thin ice to the north of Siberia (Figure 3b).

Hydrographic fields are presented in Figure 4. High salinities (>35 psu) in the Norwegian and the western Barents Seas indicate the inflow of Atlantic water from the south (Figure 4, a and c). In the Arctic Ocean proper, salinities are much lower with minima in the Siberian shelf seas due to inflowing river water. Low-saline shelf waters are advected into the central Arctic Ocean, eventually leaving the Arctic Ocean through Fram Strait or the Canadian Archipelago. The southward flow of polar water in the EGC causes low salinities in the western Nordic Seas. In the central Canadian Basin we find modelled surface salinities to be somewhat higher than observed values, resulting in a local salinity maximum which has no counterpart in observational data (EWG, 1997). This is a common and still unsolved problem in prognostic Arctic Ocean modelling (Steele *et al.*, 2001). In the depth range between 80 m and 250 m we find a salinity minimum in the Canadian Basin (Figure 4c) which is in good agreement with observations. The salinity minimum results from depressed isohalines in the Beaufort Gyre due to Ekman convergence.

The distribution of Arctic river water in the top 80 m is shown in Figure 4b. Contour labels correspond to the fraction of Arctic river water in sea water, i.e., Arctic river-water concentration. The pattern of the field resembles that of salinity over wide areas, where high river-water concentrations are associated with low salinities. As expected, we find maximum concentrations in the Siberian shelf seas. From there the water is advected towards the outlets of the Arctic Ocean. In Fram Strait the concentration of Arctic river water is about 7%, and even in northwestern Atlantic surface waters it is larger than 1%. Arctic river water is absent in the Norwegian and Chukchi Seas, which are dominated by inflowing waters from the Atlantic and Pacific, respectively. The model results are in good agreement with river-water distributions inferred from measurements of stable oxygen isotopes in Arctic sea water. The 'observational' data show high concentrations in the Kara, Laptev and Beaufort Seas, and minimum values in the Barents Sea (e.g., Frank, 1996; Schlosser *et al.*, 1999). High fractions are also found in the TPD, where concentrations of meteoric water reach up to 15% at the surface, but strongly decrease with depth, being approximately 4% at 100 m (Bauch *et al.*, 1995; Ekwurzel *et al.*, 2001).

Figure 4d shows potential temperatures at 80–250 m depths. While surface temperatures in the central Arctic Ocean are at the

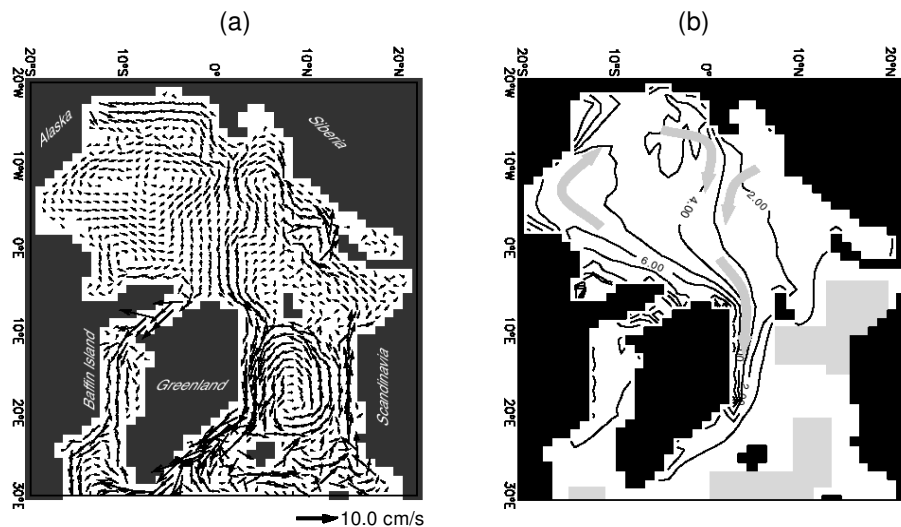


Figure 3 Present-day run (experiment PD). (a) Annual mean upper ocean velocity (averaged over 0–80 m). (b) Annual mean sea-ice thickness (m) with the mean ice-drift pattern indicated by arrows. Regions of strong convective activity in the ocean are marked by shaded areas. Labels refer to the rotated model grid.

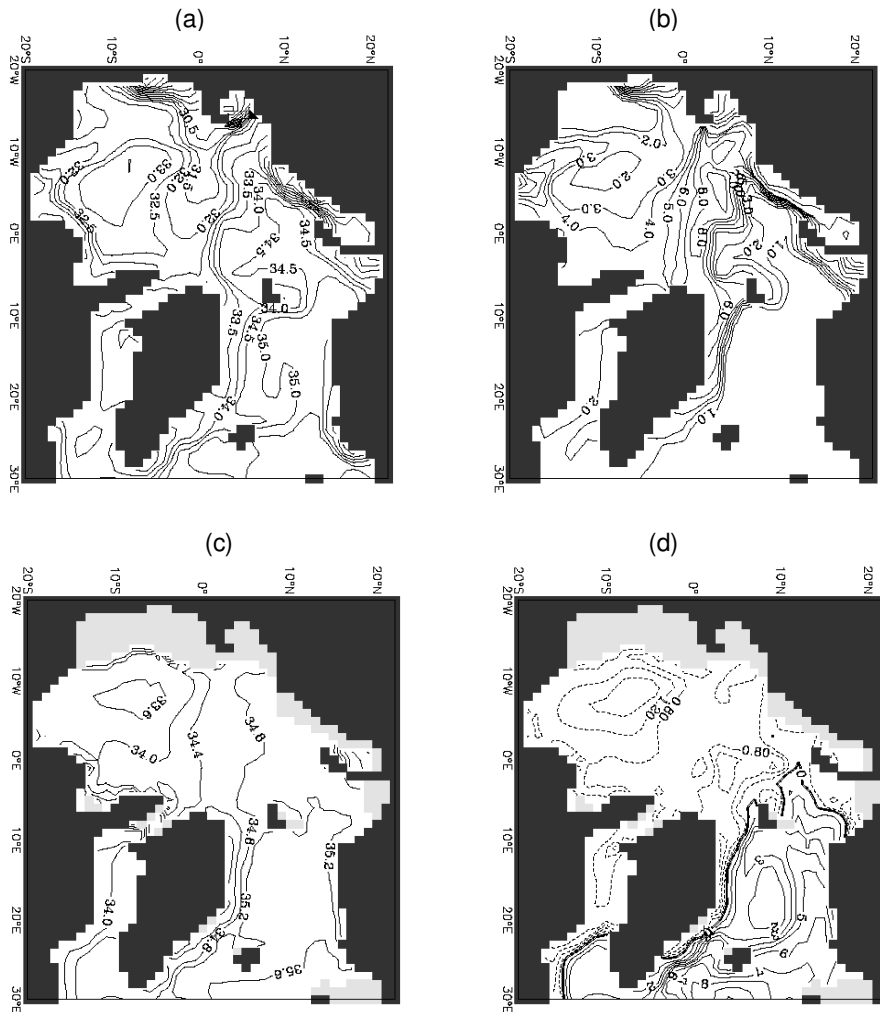


Figure 4 Annual mean hydrographic fields in the present-day run (experiment PD). (a) Salinity (psu) averaged over 0–80 m. (b) Arctic river-water concentration (%) averaged over 0–80 m. (c) Salinity (psu) averaged over 80–250 m. (d) Potential temperature (°C) averaged over 80–250 m. Labels refer to the rotated model grid.

freezing point (not shown), we notice the heating effect of warm Atlantic water masses in subsurface layers. The temperature minimum in the central Canadian Basin results from Ekman convergence in the Beaufort Gyre. Annual mean temperatures above 0°C can be found in the Barents Sea and in the eastern Fram Strait as a result of Atlantic water flowing into the Arctic Ocean.

Mid-Holocene experiment (MH)

The most notable feature of the freshwater forcing in experiment MH is a massive river input to the Laptev Sea. This freshwater supply is conspicuous in Figure 5a, which shows differences in mean upper ocean salinity between experiment MH and experiment PD. A zone of relatively low salinity extends from the Laptev Sea to Fram Strait and beyond. Salinities lower than today appear in the East Siberian Sea due to enhanced local runoff, whereas a smaller local freshwater inflow gives rise to higher salinities in the Kara Sea (cf. Table 1).

Differences in mean potential temperature between experiment MH and experiment PD are presented in Figure 5b for the depth range 80–250 m. Largest values naturally appear in the ‘high-temperature’ North Atlantic. Yet also in the Arctic Ocean we find differences up to 1°C, which is enormous in view of the low temperatures there. In the central Arctic, these differences can be explained by changes in salinity (i.e., density) stratification rather than by horizontal advection. Low surface salinities stabilize the water-column, thereby inhibiting convective mixing of cold surface water with warmer water from deeper halocline layers.

Changes in surface salinity are associated with changes in

upper-ocean velocity. Figure 5c reveals considerable differences between the two experiments, particularly in the Eurasian Basin and the EGC. In experiment MH, we find an increased through-flow in the western Fram Strait, and weaker flow through the Canadian Archipelago. The freshening of the EGC, visible in Figure 5a, is associated with a stronger surface current. Thus it appears that the EGC is, at least partially, driven by freshwater-induced density gradients (cf. Wadhams *et al.*, 1979).

Differences in sea-ice thickness between experiment MH and experiment PD are shown in Figure 5d. Thicker ice in experiment MH north of Greenland is primarily due to a more convergent ice drift. The drift of sea ice is coupled with ocean currents through ocean/sea-ice stresses. Therefore, differences in sea-ice motion between the experiments are almost identical to differences in the upper-ocean circulation displayed in Figure 5c.

The model integration time of 60 years would be long enough for anomalous Arctic freshwater input to affect the large-scale Atlantic thermohaline circulation through an influence on convection and deep-water formation in the Nordic Seas and the North Atlantic (Gerdes and Köberle, 1995; Prange and Gerdes, 1999). Calculation of the Atlantic meridional overturning, however, reveals that the different freshwater forcings in experiments PD and MH do not result in major changes of the thermohaline circulation. Pattern and strength of the meridional overturning circulations are almost identical in the two experiments (not shown). The differences in total Arctic freshwater input appear to be too small to exert a noticeable influence on the Atlantic thermohaline circulation, as they hardly affect the important convective regions

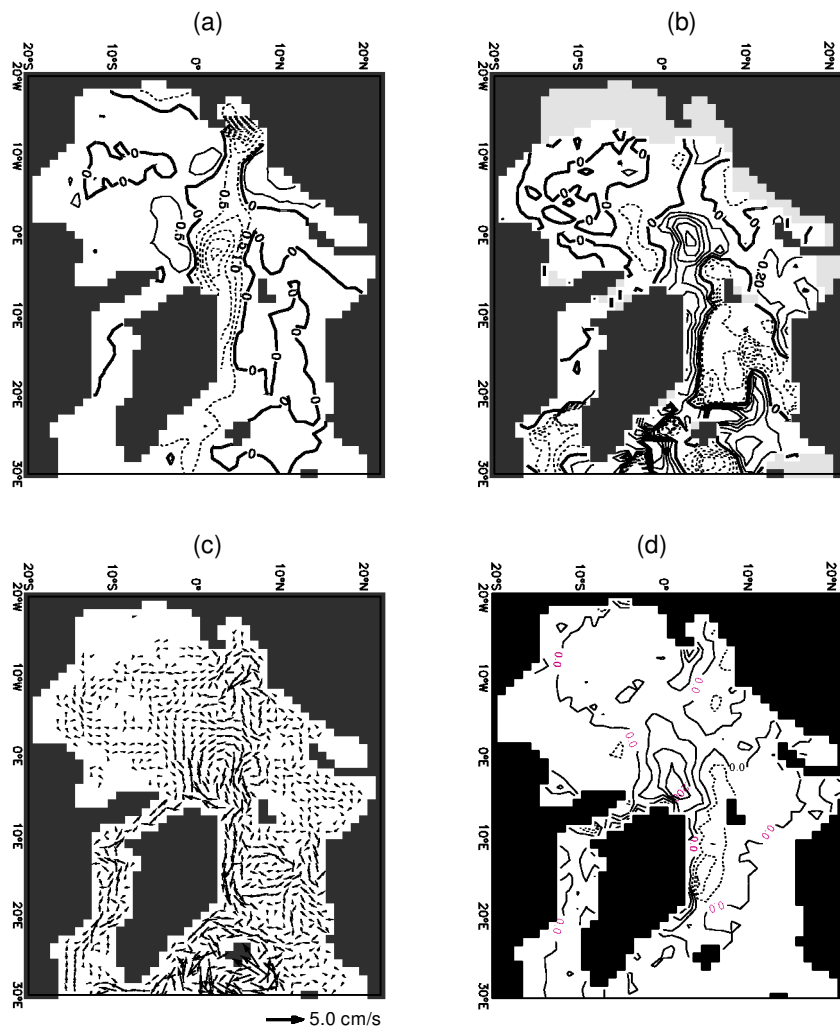


Figure 5 Differences in mean fields between experiment MH and experiment PD (i.e., MH–PD). (a) Salinity (psu) averaged over 0–80 m. (b) Potential temperature (°C) averaged over 80–250 m. (c) Upper ocean velocity averaged over 0–80 m. (d) Sea-ice thickness (contour interval is 0.1 m). Labels refer to the rotated model grid.

in the Norwegian, Barents and Greenland Seas marked in Figure 3b by the shaded areas.

Discussion

Variations in the TPD during the Holocene were hypothesized by Dyke *et al.* (1997) from radiometric analyses of driftwood collected in the Canadian Archipelago. Driftwood from the boreal forests reaches the Arctic Ocean from North America and Eurasia. The authors interpreted changes in wood delivery to the Canadian Archipelago and Baffin Bay as resulting from changes in the path of the TPD. When the TPD was deflected westward, wood was delivered widely to the coasts of the Canadian Archipelago; when the TPD exited entirely through Fram Strait, only a small amount of wood was carried to the northern coasts of the archipelago, but some was transported into Baffin Bay via the EGC and the West Greenland Current. The driftwood record comprises the last 8.5 (radiocarbon) ka and suggests two time intervals of increased Fram Strait outflow associated with an eastward shift of the TPD: 6.75–6 ka BP and 5.25–5 ka BP.

Tremblay *et al.* (1997) hypothesized that changes in the wind forcing were responsible for the inferred variations in the upper-ocean and sea-ice circulation patterns. Utilizing a dynamic-thermodynamic sea-ice model, the authors demonstrated the effect

of different wind-stress patterns on the large-scale Arctic ice drift. Depending on the position of sea-level isobars over the Arctic Ocean, export of sea ice through Fram Strait is favoured or diminished. However, there is no further evidence for such variations in the palaeoatmospheric circulation over the Arctic Ocean that could support the hypothesis of Tremblay *et al.* (1997).

The results of the present study reveal the importance of freshwater input on the Arctic upper-ocean and sea-ice circulation, thus providing an alternative or complementary explanation for the changes in the path of the TPD. Compared to the present-day simulation (experiment PD), the freshwater forcing of the time interval around 6 ka BP (experiment MH) results in a modified path of the TPD, shifted to the east with enhanced transports through Fram Strait and reduced flow through the Canadian Archipelago (Figure 5c). This flow pattern is consistent with the circulation pattern inferred by Dyke *et al.* (1997) for the time interval between 6.75 and 6 ka BP.

Our model results point to a direct connection between Siberian river runoff and the path of the TPD. It is possible that an eastward shift of the TPD during the time interval 5.25–5 ka BP (Dyke *et al.*, 1997) was also associated with enhanced Siberian runoff. Indeed, an increased abundance of freshwater algae has been found in sediment cores from the Kara Sea and the Eurasian continental margin for the time around 5 ka BP (Boucsein, 2000).

Conclusions and outlook

Using geological evidences for the circum-Arctic palaeoriver run-off of the time interval around 6 ka BP, our model reveals strong changes in the polar oceanic circulation associated with the mid-Holocene freshwater forcing. In contrast to Arctic Ocean variations on interannual timescale, which are governed primarily by wind-stress fluctuations over the sea (e.g., Zhang *et al.*, 1999), the circulation pattern is largely controlled by freshwater input from the surrounding continents on longer timescales. We suggest that long-term Holocene variability in Arctic freshwater forcing had the potential to cause considerable variability in Arctic Ocean dynamics on a century-to-millennium timescale.

In the future, we expect to gain more insight into the past Arctic freshwater budget by utilizing coupled climate models. Recent efforts in palaeoclimate modelling intercomparison, however, showed considerable discrepancies among the various models in use concerning mid-Holocene *P–E* in high latitudes (cf. Yu and Harrison, 1996; de Noblet *et al.*, 2000). Although the hydrological cycle with its characteristically small spatial scales is notoriously difficult to obtain, it is important for the Arctic Ocean flow field and the associated freshwater transports through Fram Strait and the Canadian Archipelago.

In the present study, we investigated the influence of Arctic freshwater forcing on the coupled ocean/sea-ice system, isolated from any other effects. Examining the dynamical impact of varying atmospheric forcing and ocean-bottom topography, acting both separately and in concert, would be the logical next step towards understanding Arctic Ocean variability during the Holocene.

Acknowledgements

We thank R. Gerdes and K. Herterich for their continued support. Comments by J.-H. Kim and an anonymous reviewer helped to improve the paper. We kindly acknowledge financial support from the German Federal Ministry for Education, Science and Research (BMBF) through the KIHZ and DEKLIM projects.

References

Aagaard, K. and Carmack, E.C. 1989: The role of sea ice and other freshwater in the Arctic circulation. *Journal of Geophysical Research* 94, 14485–98.

AANII 1990: Estimate of river inflow to the Karsk Sea and its annual and seasonal variation. AANII Report, Leningrad (St Petersburg): Arctic and Antarctic Research Institute, 107 pp.

Andreev, A.A. and Klimanov, V.A. 2000: Quantitative Holocene climate reconstruction from Arctic Russia. *Journal of Paleolimnology* 24, 81–91.

Bauch, D., Schlosser, P. and Fairbanks, R.G. 1995: Freshwater balance and the sources of deep and bottom waters in the Arctic Ocean inferred from the distribution of $H_2^{18}O$. *Progress in Oceanography* 35, 53–80.

Behrends, M. 1999: Rekonstruktion von Meereisdrift und terrigenem Sedimenteintrag im Spätquartär: Schwerminerallasoziationen in Sedimenten des Laptev-See-Kontinentalrandes und des zentralen Arktischen Ozeans. *Reports on Polar Research* 310, Bremerhaven: Alfred Wegener Institute for Polar and Marine Research, 167 pp.

Belyaev, A.V. and Georgiadi, A.G. 1992: Annual mean runoff during the Last Interglacial and Holocene climatic optima. In Frenzel, B., Peccsi, M. and Velichko, A.A., editors, *Atlas of paleoclimates and paleoenvironments of the Northern Hemisphere: Late Pleistocene–Holocene*, Geographical Research Institute, Hungarian Academy of Sciences, Stuttgart: Gustav Fischer Verlag, 140–41.

Boucsein, B. 2000: Organic carbon in Late Quaternary sediments: responses to paleoenvironmental changes in the Laptev and Kara Seas (Arctic Ocean). *Reports on Polar Research* 365, Bremerhaven: Alfred Wegener Institute for Polar and Marine Research, 103 pp.

Bourke, R. and Garrett, C. 1987: Sea-ice thickness distribution in the Arctic Ocean. *Cold Regions Science and Technology* 13, 259–80.

Bourke, R.H. and McLaren, A.S. 1992: Contour mapping of Arctic Basin ice draft and roughness parameters. *Journal of Geophysical Research* 97, 17715–28.

Chapman, W. L., Welch, W., Bowman, K.P., Sacks, J. and Walsh, J.E. 1994: Arctic sea ice variability: model sensitivities and a multidecadal simulation. *Journal of Geophysical Research* 99, 919–35.

Cheddadi, R., Yu, G., Guiot, J., Harrison, S.P. and Prentice, I.C. 1997: The climate of Europe 6000 years ago. *Climate Dynamics* 13, 1–9.

Cronin, T.M., Holtz, T.R. Jr, Stein, R., Spielhagen, R., Fütterer, D. and Wollenburg, J. 1995: Late Quaternary paleoceanography of the Eurasian Basin, Arctic Ocean. *Paleoceanography* 10, 259–81.

de Noblet, N., Bartlein, P. and Bonfils, C. 2000: Simulated and observed changes in the extratropics during the mid-Holocene. Proceedings, 3rd PMIP Workshop, Paleoclimate Modelling Intercomparison Project, La Huardière, Canada, October 1999, *World Climate Research Programme (WCRP)* 111, 69–76.

Dukowicz, J.K. and Smith, R.D. 1994: Implicit free-surface method for the Bryan-Cox-Semtner Ocean Model. *Journal of Geophysical Research* 99, 7991–8014.

Dyke, A.S., England, J., Reimnitz, E. and Jette, J. 1997: Changes in driftwood delivery to the Canadian Arctic Archipelago: the hypothesis of postglacial oscillations of the Transpolar Drift. *Arctic* 50, 1–16.

Ekwurzel, B., Schlosser, P., Mortlock, R., Fairbanks, R. and Swift, J.H. 2001: River runoff, sea ice meltwater, and Pacific water distribution and mean residence times in the Arctic Ocean. *Journal of Geophysical Research* 106, 9075–92.

EWG (Environmental Working Group) 1997: Joint U.S.–Russian atlas of the Arctic Ocean. Boulder, CO: National Snow and Ice Center, CD-ROM.

Frank, M. 1996: Spurenstoffuntersuchungen zur Zirkulation im Eurasischen Becken des Nordpolarmeeres. PhD thesis, Heidelberg: Ruprecht-Karls-Universität, 100 pp.

Gerdes, R., Köberle, C. and Willebrand, J. 1991: The influence of numerical advection schemes on the results of ocean general circulation models. *Climate Dynamics* 5, 211–26.

Gerdes, R. and Köberle, C. 1995: On the influence of DSOW in a numerical model of the North Atlantic general circulation. *Journal of Physical Oceanography* 25, 2624–42.

Grabs, W., De Couet, T. and Pauler, J. 1996: Freshwater fluxes from continents into the world oceans based on data of the Global Runoff Data Base. *GRDC Report* 10, Koblenz: Global Runoff Data Centre, Federal Institute of Hydrology, 228 pp.

Harder, M. 1996: Dynamik, Rauhigkeit und Alter des Meereises in der Arktis – Numerische Untersuchungen mit einem großskaligen Modell. *Reports on Polar Research* 203, Bremerhaven: Alfred Wegener Institute for Polar and Marine Research, 126 pp.

Hibler, W.D. III 1979: A dynamic-thermodynamic sea ice model. *Journal of Physical Oceanography* 9, 815–46.

Kunz-Pirrung, M. 1998: Rekonstruktion der Oberflächenwassermassen der östlichen Laptevsee im Holozän anhand von aquatischen Palynomorphen. *Reports on Polar Research* 281, Bremerhaven: Alfred Wegener Institute for Polar and Marine Research, 117 pp.

Lubinski, D.J., Polyak, L. and Forman, S.L. 2001: Freshwater and Atlantic water inflows to the deep northern Barents and Kara seas since ca 13 ^{14}C ka. *Quaternary Science Reviews* 20, 1851–79.

Monserud, R.A., Tchekakova, N.M. and Denissenko, O.V. 1998: Reconstruction of the mid-Holocene palaeoclimate of Siberia using a bioclimatic vegetation model. *Palaeogeography, Palaeoclimatology, Palaeoecology* 139, 15–36.

Pacanowski, R.C. 1995: MOM 2 Documentation (user's guide and reference manual). *Geophysical Fluid Dynamics Laboratory (GFDL) Ocean Technical Report* 3, Princeton, NJ: Princeton University, 232 pp.

Plitkin, G.A. 1978: Inflow of surface waters into Siberian and Far Eastern seas and method of calculating it in individual years. *Water Resources* 5, 211–19.

Polyak, L., Levitan, M., Gataullin, V., Khusid, T., Mikhailov, V. and Mukhina, V. 2000: The impact of glaciation, river-discharge and sea-level change on Late Quaternary environments in the southwestern Kara Sea. *International Journal of Earth Science* 89, 550–62.

Polyak, L., Levitan, M., Khusid, T., Merklin, L. and Mukhina, V. 2002: Variations in the influence of riverine discharge on the Kara Sea

- during the last deglaciation and the Holocene. *Global and Planetary Change* 32, 291–309.
- Prange, M.** 2003: Einfluss arktischer Süßwasserquellen auf die Zirkulation im Nordmeer und im Nordatlantik in einem prognostischen Ozean-Meereis-Modell. To appear in *Reports on Polar and Marine Research*, Bremerhaven: Alfred Wegener Institute for Polar and Marine Research.
- Prange, M.** and **Gerdes, R.** 1999: Influence of Arctic river runoff on the circulation in the Arctic Ocean, the Nordic Seas and the North Atlantic. *International Council for the Exploration of the Seas – Council Meeting (ICES-CM)* 1999/L:11, 5 pp.
- Roach, A.T., Aagaard, K., Pease, C.H., Salo, S.A., Weingartner, T., Pavlov, V.** and **Kulakov, M.** 1995: Direct measurements of transport and water properties through the Bering Strait. *Journal of Geophysical Research* 100, 18443–57.
- Roeske, F.** 2001: An atlas of surface fluxes based on the ECMWF reanalysis – a climatological dataset to force global ocean general circulation models. *Max Planck Institute Report* 323, Hamburg: Max Planck Institute for Meteorology, 31 pp.
- Rudels, B., Anderson, L.G.** and **Jones, E.P.** 1996: Formation and evolution of the surface mixed layer and halocline of the Arctic Ocean. *Journal of Geophysical Research* 101, 8807–21.
- Schlosser, P., Bayer, R., Bönisch, G., Cooper, L., Ekwurzel, B., Jenkins, W.J., Khatiwala, S., Pfirman, S.** and **Smethie, W.M.** 1999: Pathways and mean residence times of dissolved pollutants in the ocean derived from transient tracers and stable isotopes. *The Science of the Total Environment* 237/238, 15–30.
- Steele, M.** and **Boyd, T.** 1998: Retreat of the cold halocline layer in the Arctic Ocean. *Journal of Geophysical Research* 103, 10419–35.
- Steele, M., Ermold, W., Häkkinen, S., Holland, D., Holloway, G., Karcher, M., Kauker, F., Maslowski, W., Steiner, N.** and **Zhang, J.** 2001: Adrift in the Beaufort Gyre: a model intercomparison. *Geophysical Research Letters* 28, 2935–38.
- Stein, R.** and **Fahl, K.** 2000: Holocene accumulation of organic carbon at the Laptev Sea continental margin (Arctic Ocean): sources, pathways, and sinks. *Geo-Marine Letters* 20, 27–36.
- Tartinville, B., Campin, J.M., Fichefet, T.** and **Goosse, H.** 2001: Realistic representation of the surface freshwater flux in an ice-ocean general circulation model. *Ocean Modelling* 3, 95–108.
- Tremblay, L.-B., Mysak, L.A.** and **Dyke, A.S.** 1997: Evidence from driftwood records for century-to-millennial scale variations of the high latitude atmospheric circulation during the Holocene. *Geophysical Research Letters* 24, 2027–30.
- Treshnikov, A.F.**, editor 1985: *Arctic atlas*. Moscow: Arctic-Antarctic Nauchno-Issled. Institute, 204 pp.
- Vuglinsky, V.S.** 1997: River water inflow to the Arctic Ocean – conditions of formation, time variability and forecasts. Proceedings, Conference on Polar Processes and Global Climate, Rosario, Washington, November 1997, Int. ACSYS Project Office, 275–76.
- Wadhams, P., Gill, A.E.** and **Linden, P.F.** 1979: Transects by submarine of the East Greenland Polar Front. *Deep-Sea Research* 26A, 1311–27.
- Yu, G.** and **Harrison, S.P.** 1996: An evaluation of the simulated water balance of Eurasia and northern Africa at 6000 y BP using lake status data. *Climate Dynamics* 12, 723–35.
- Zalesak, S.T.** 1979: Fully multidimensional flux-corrected transport algorithms for fluid. *Journal of Computational Physics* 31, 335–62.
- Zhang, Y., Maslowski, W.** and **Semtner, A.J.** 1999: Impact of mesoscale ocean currents on sea ice in high resolution Arctic ice and ocean simulations. *Journal of Geophysical Research* 104, 18409–29.